

Mapping the phase diagram of the quantum anomalous Hall and topological Hall effects in a dual-gated magnetic topological insulator heterostructure

Run Xiao^{†,1}, Di Xiao^{†,1}, Jue Jiang^{†,1}, Jae-Ho Shin,¹ Fei Wang,¹ Yi-Fan Zhao,¹
Ruo-Xi Zhang,¹ Anthony Richardella,^{1,2} Ke Wang,² Morteza Kayyalha,³
Moses H. W. Chan,¹ Chao-Xing Liu,¹ Cui-Zu Chang,^{1,*} and Nitin Samarth^{1,*}

¹*Department of Physics, The Pennsylvania State University, University Park PA 16802*

²*Materials Research Institute, The Pennsylvania State University, University Park PA 16802*

³*Department of Electrical Engineering,*

The Pennsylvania State University, University Park PA 16802

(Dated: March 12, 2021)

Abstract

We use magnetotransport in dual-gated magnetic topological insulator heterostructures to map out a phase diagram of the topological Hall and quantum anomalous Hall effects as a function of the chemical potential (primarily determined by the back gate voltage) and the asymmetric potential (primarily determined by the top gate voltage). A theoretical model that includes both surface states and valence band quantum well states allows the evaluation of the variation of the Dzyaloshinskii-Moriya interaction and carrier density with gate voltages. The qualitative agreement between experiment and theory provides strong evidence for the existence of a topological Hall effect in the system studied, opening up a new route for understanding and manipulating chiral magnetic spin textures in real space.

In recent years, condensed matter physics has seen a growing interest in studying the interplay between topology in momentum space and topology in real space. The former often manifests in nontrivial band structures in momentum space arising from the combined effects of some fundamental symmetry and strong spin-orbit coupling, while the latter (also a product of spin-orbit coupling) is associated with chiral magnetic spin textures in real space [1–3]. The quantum anomalous Hall (QAH) effect [4–12], induced by a non-trivial Berry curvature in a topological system with broken time-reversal symmetry, provides convincing evidence of topology in momentum space. It is characterized by a quantized Hall resistance and a vanishing longitudinal resistance at zero magnetic field and has been realized in magnetically doped topological insulators (TIs) [8–12]. The topological Hall effect (THE), induced by the interaction of itinerant charge carriers with chiral spin textures such as magnetic skyrmions or chiral domain walls, is regarded as a signature of topology in real space [3]. The THE manifests as an excess Hall voltage superimposed on the usual hysteretic anomalous Hall voltage that arises in magnetic conductors. Such a signature has been observed and interpreted as evidence for the THE in many systems, including MnSi [13, 14], MnGe [15], FeGe [16], SrIrO₃/SrRuO₃ interface [17, 18], magnetically doped TI heterostructures [19–21], and TI/BaFe₁₂O₁₉ heterostructures [22]. Given this context, it is valuable to identify model systems wherein the QAH and THE can be systematically studied as a function of some easily tuned system parameters. We recently studied the THE in one such model system, TI sandwich heterostructures of (Cr_{0.15}(Bi,Sb)_{1.85}Te₃ - (Bi,Sb)₂Te₃

* Corresponding authors: nsamarth@psu.edu, cxc955@psu.edu

- $\text{Cr}_{0.15}(\text{Bi,Sb})_{1.85}\text{Te}_3$, referred as CBST-BST-CBST below) [23]. By using a bottom gate to tune the chemical potential, we showed how a single sample could be continuously tuned from the QAH effect regime to the THE regime.

In this *Letter*, we further extend the tunability of this model system by adding a top gate and demonstrate how a dual gating scheme enables the mapping of a phase diagram of the concurrence of the QAH effect and the THE as a function of the chemical potential and the asymmetry in the potential between the top and bottom surfaces. In particular, we find that the THE is enhanced when top and bottom gate voltages have different signs and that it is quenched when these gate voltages have the same sign. We also demonstrate that the THE arises because the asymmetric potential induced by dual gates leads to a Dzyaloshinskii-Moriya (DM) interaction.

We used a VEECO 620 molecular beam epitaxy system to grow 3 quintuple layer (QL) CBST - 5QL BST - 3QL CBST heterostructures on SrTiO_3 (111) substrates (MTI Corporation). The SrTiO_3 substrates were first soaked in deionized water at 90°C for 1.5 hours and thermally annealed at 985°C for 3 hours in a tube furnace with flowing oxygen gas. The heat-treated SrTiO_3 substrates were then outgassed under vacuum at 630°C (thermocouple temperature) for 1 hour. After outgassing, the substrates were cooled down to 340°C (thermocouple temperature) for the heterostructure growth. High purity Cr (5 N), Bi (5 N), Sb (6 N), and Te (6 N) were evaporated from Knudsen effusion cells. The cell temperatures were precisely controlled to obtain the desired beam equivalent pressure (BEP) fluxes of each element. The BEP flux ratio of $\text{Te}/(\text{Bi}+\text{Sb})$ was higher than 10 to prevent Te deficiency. The BEP flux ratio of Sb/Bi was around 2 to tune the heterostructure's chemical potential close to the charge neutral point. The heterostructure growth rate was ~ 0.25 QL/min, and the pressure of the MBE chamber was maintained at 2×10^{-10} mbar during the growth.

After the growth, the heterostructures were capped with 10 nm Te *in situ* at 20°C for protection during the fabrication process. Heterostructures were then fabricated into Hall bar devices using photolithography and Ar^+ plasma dry etching. The top gate was defined by a 40 nm Al_2O_3 dielectric layer and 5nm Ti/50nm Au contacts deposited by atomic layer deposition and electron beam evaporation, respectively.

We carried out magnetotransport measurements in a commercial He3 fridge (Oxford Heliox) for temperatures higher than 0.4 K and in a commercial Leiden Cryogenics dilution refrigerator at $T = 60$ mK. Bottom and top gate voltages were applied using the SrTiO_3

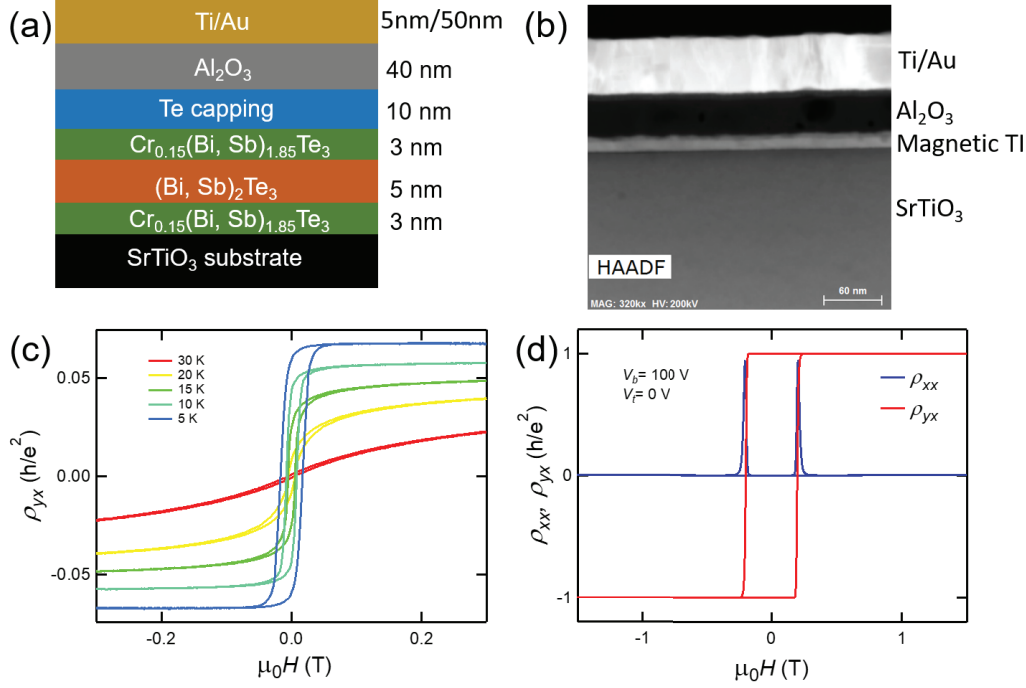


FIG. 1. The QAH effect in dual-gated magnetic TI heterostructures. (a) A schematic structure of the magnetic TI heterostructure. The compositions of the layers are nominal and based on past calibrations of sample growth. (b) Cross-sectional TEM image of a dual-gated device. (c) Temperature variation of the magnetic field dependence of Hall resistance. (d) Demonstration of the QAH effect at $T = 60$ mK with gate voltages $V_b = 100$ V and $V_t = 0$ V.

substrate and the deposited Al₂O₃ layer as the dielectric layers.

Figures 1(a) and (b) show the detailed schematic structure and a cross-sectional transmission electron microscope (TEM) image, respectively, of one sample we studied. The sandwich heterostructure geometry consists of two ultrathin (3 QL) magnetic TI layers separated by a non-magnetic TI layer and has been shown to improve the quality of the observed QAH effect at higher temperatures (up to 2 K)[12]. More important for the purposes of this paper, since the magnetic TI layers are separated by a non-magnetic TI, the magnetic exchange interaction between top and bottom layers is weakened. This allows for a significant DM interaction, which is a requirement for the THE [3]. Figure 1(c) shows the temperature dependence of anomalous Hall effect. A hysteresis loop develops below a Curie temperature around 20 K. As the sample is cooled down to the base temperature at $T = 60$ mK, a robust QAH effect develops depending on the values of the top and bottom gate voltages ($V_b=100$

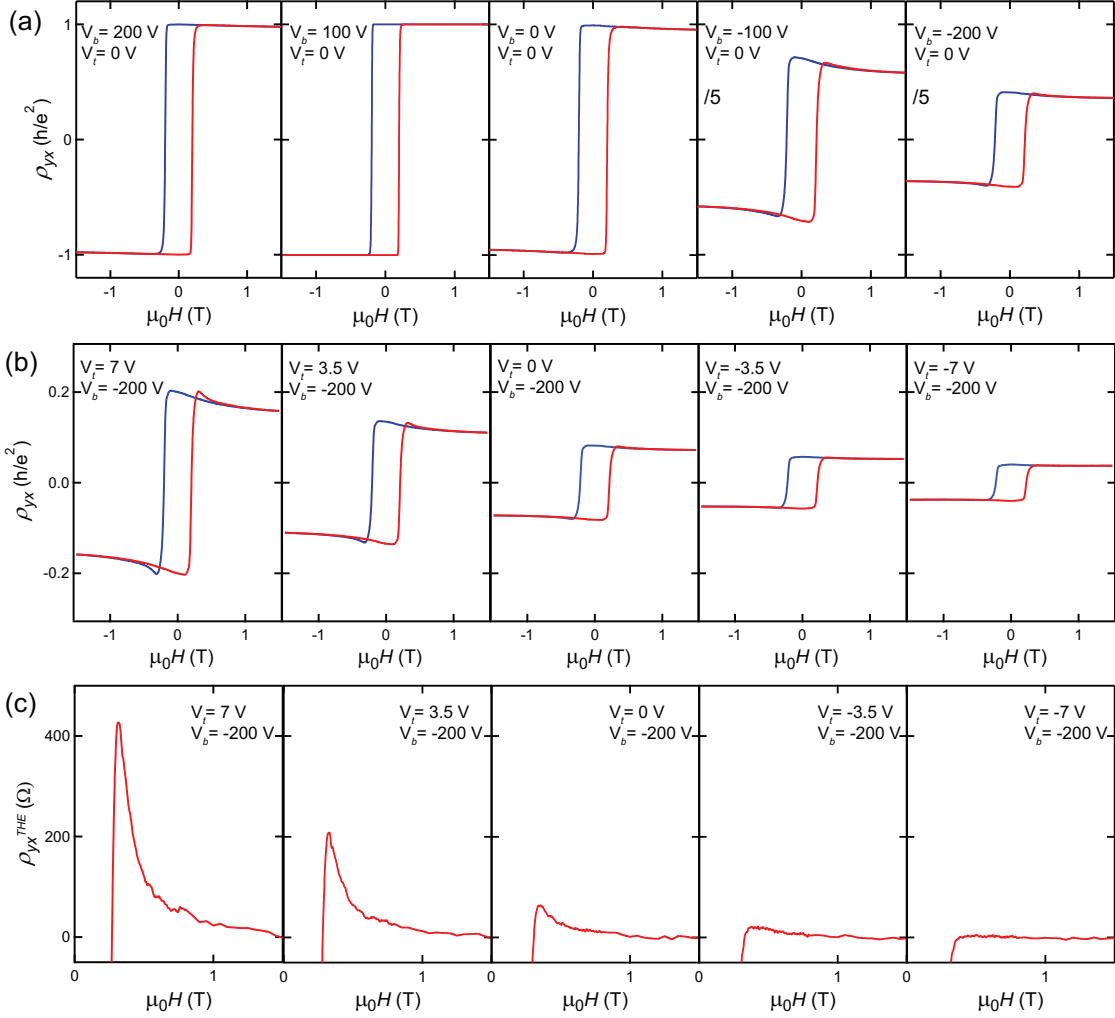


FIG. 2. The topological Hall effect observed in dual-gated magnetic TI heterostructures. (a) The deviation from the QAH regime using the bottom gate. (b) Top gate-voltage-driven THE. The bottom gate voltage V_b is fixed at -200V. By applying a positive top gate voltage V_t , the THE becomes more pronounced. On the other hand, applying a negative V_t can make the THE vanish. (c) Top gate voltage dependence of the magnitude of the THE ρ_{yx}^{THE} . The data are obtained by subtracting a constant high field Hall resistance.

V , $V_t=0$ V in Figs. 1 (d)).

At the base temperature $T = 60$ mK, we mapped out the top and bottom gate voltage dependence of the QAH effect and the THE. As shown in Fig. 2(a), if the bottom gate V_b is changed while the top gate V_t is fixed at 0 V, the heterostructure can be tuned away from the QAH regime, particularly at negative V_b . Away from the QAH regime, at magnetic

fields larger than the coercive field, a careful examination of the Hall resistance shows that it is slightly different during the upward and downward magnetic field sweeps. The excess Hall resistance after crossing the magnetic reversal transition is a signature of the THE. Therefore, by tuning V_b , we observe a crossover from the QAH effect to the THE. This is due to the formation of chiral domain walls in the presence of a strong DM interaction [23].

The signature of the THE becomes more obvious if we apply a positive V_t while keeping V_b fixed at a negative value (Fig. 2(b)). If we fix V_b and change V_t , the THE behaves differently: unlike the case of V_b -modulated THE, it becomes more pronounced at positive V_t but vanishes under negative V_t . In Fig. 2(c), we plot the gate voltage dependence of the magnitude of the THE, obtained by subtracting the Hall voltage measured during the upward and downward sweeps of the magnetic field (ρ_{yx}^{THE}). This allows us to observe the variation of the QAH effect and the THE as a function of the chemical potential. The maximum of ρ_{yx}^{THE} occurs when V_t and V_b have different signs. In contrast, when they have the same sign, ρ_{yx}^{THE} decreases and vanishes.

In order to understand the behavior of the THE, we propose a simple capacitance model (Fig. 3(a)). The top and bottom gates act as capacitors that inject or repel electrons in the top and bottom surfaces, respectively. Therefore, the top gate chiefly tunes the chemical potential of the top surface, while the bottom gate principally affects the chemical potential of the bottom surface. As a result, an asymmetric potential between top and bottom surfaces is induced, leading to the breaking of inversion symmetry in the sandwich heterostructure. Due to the broken inversion symmetry, the overall DM interaction from two surface is non-zero, giving rise to the THE.

As shown in Fig. 3(b), the sandwich heterostructure enters the QAH effect regime in the dark blue area. In this region of the phase diagram, conduction from surface and bulk carriers is minimized; thus, the sample shows a perfect QAH effect with no THE signal. Away from the QAH regime where surface carriers start to contribute, a finite DM interaction is induced, and the THE appears. Furthermore, by creating an asymmetric potential by V_b and V_t , ρ_{yx}^{THE} reaches maximum shown in the red area.

We now theoretically evaluate the DM interaction and the bulk carrier concentrations in magnetic TI heterostructures based on the model developed in Ref. [23]. This model involves both the topological surface states and the bulk valence band quantum well states, both of which have been shown to be crucial in understanding the temperature and chemical

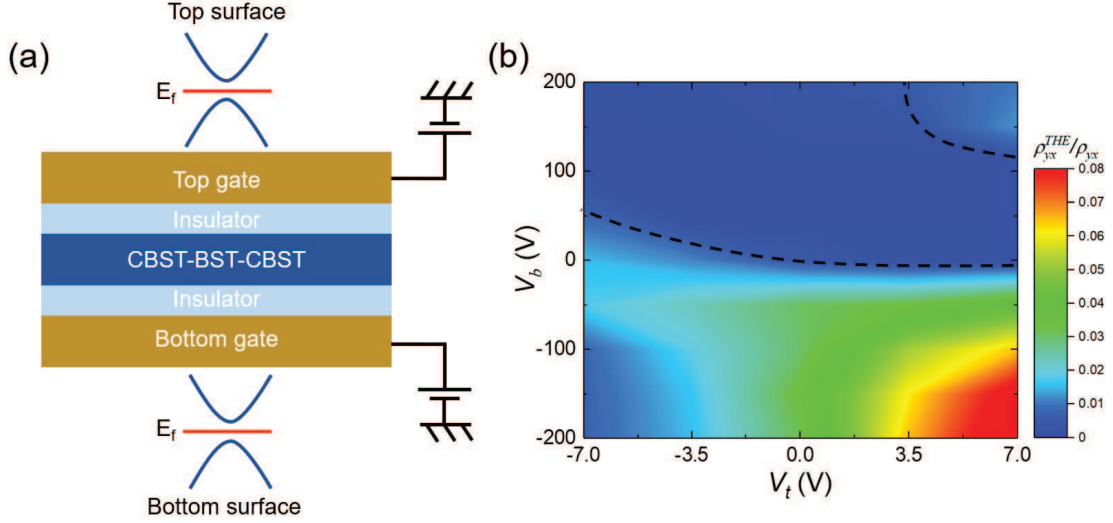


FIG. 3. The gate voltage dependence of the THE. (a) Capacitance model of the gating effect. The top gate mainly tunes the chemical potential of the top surface while the bottom gate mainly tunes the chemical potential of the bottom surface. Dual gates can induce an asymmetric potential between top and bottom surfaces. (b) The THE phase diagram. THE is absent in the QAH effect regime (dark blue area). Away from the QAH regime, when the top and back gate voltages have different signs, the THE becomes more obvious (red area). When dual gates have the same sign, the THE is quenched (lower left corner).

potential dependence in the previous report [23]. The topological surface states can be described by the effective Hamiltonian $H_{SS} = v_F(k_y\sigma_x - k_x\sigma_y)\tau_z + U\tau_z + m_0\tau_x + H_{SS,ex}$, where σ is the Pauli matrices for the spin while τ stands for two surfaces. Here v_F is the Fermi velocity, U is the asymmetric potential and m_0 describes the hybridization between two surface states at the top and bottom surfaces. The exchange coupling between surface states and magnetic moments can be described by the Hamiltonian $H_{SS,ex} = -\mathbf{M}^t \cdot \sigma \frac{1+\tau_z}{2} - \mathbf{M}^b \cdot \sigma \frac{1-\tau_z}{2}$, where \mathbf{M}^t and \mathbf{M}^b label the magnetization at the top and bottom surfaces, respectively. The valence band quantum well states are described by the effective Hamiltonian $H_{QW} = \varepsilon_0(k) + N(k)\tau_z + A(k_y\sigma_x - k_x\sigma_y)\tau_x + U\tau_x + H_{QW,ex}$, where σ still labels spin and τ stands for two orbitals instead. Here $\varepsilon_0(k) = C_0 + C_1k^2$, $N(k) = N_0 + N_1k^2$ and C_0, C_1, N_0, N_1, A are material dependent parameters while U is still for the asymmetric potential. The exchange coupling between quantum well states and magnetic moments is given by $H_{QW,ex} = -\mathbf{M} \cdot \sigma$, where \mathbf{M} is the magnetization. We assume the magnetization is uniform throughout the

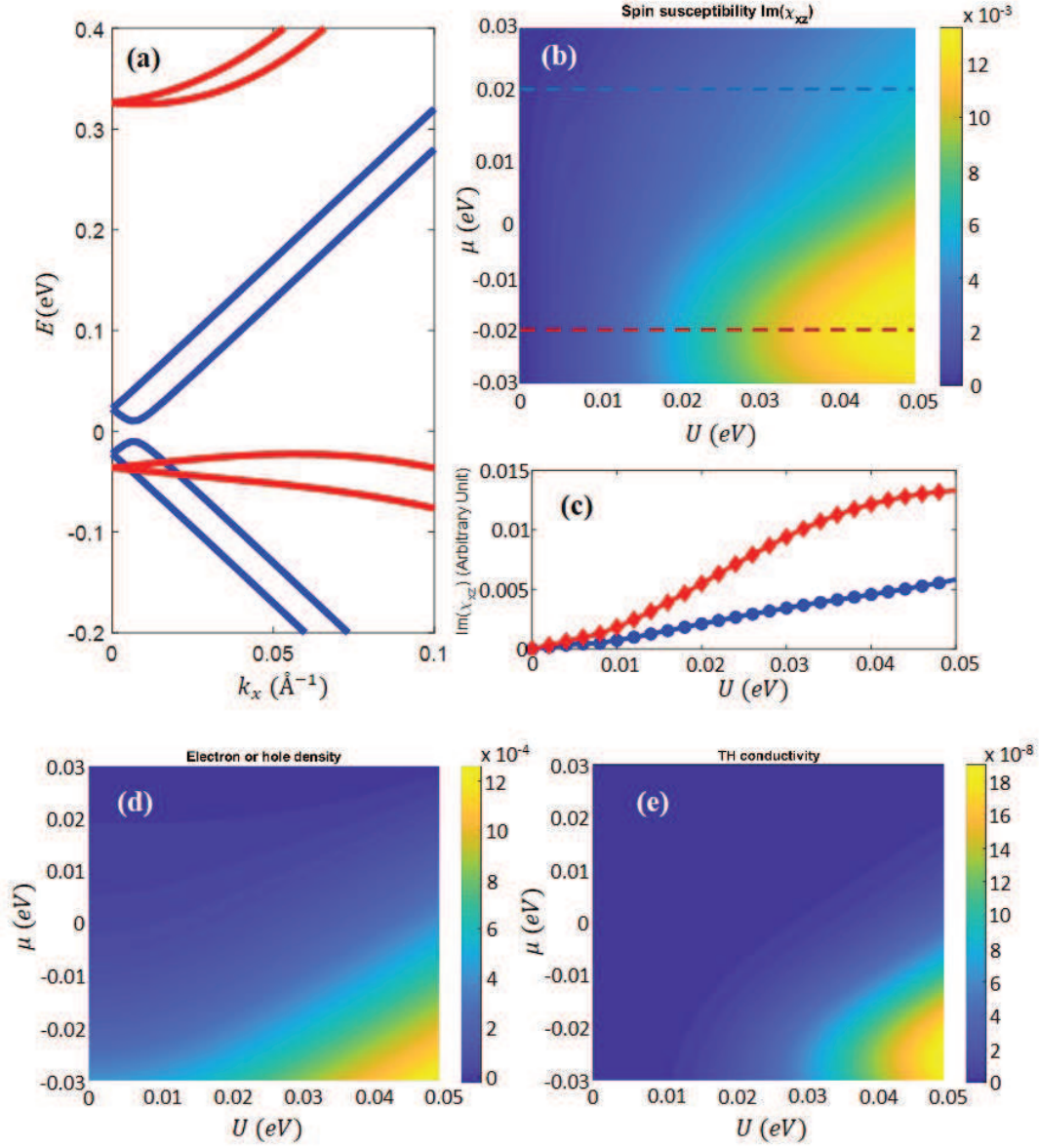


FIG. 4. (a) The energy dispersion of the surface states and bulk quantum well bands in a magnetic TI. Here $U = 0.02\text{eV}$. (b) Spin susceptibility χ_{xz} as a function of chemical potential μ and asymmetric potential U . The blue and red dashed lines correspond to the blue and red plots in (c). (c) Spin susceptibility χ_{xz} as a function of U for the chemical potential $\mu = 0.02\text{eV}$ (blue line) and $\mu = -0.02\text{eV}$ (red line). (d) Electron or hole carrier concentration ρ as a function of chemical potential μ and asymmetric potential U . Here ρ is in the unit of \AA^{-2} . The TH resistance is expected to be proportional to $|\chi_{xz}|^2\rho$, whose dependence on μ and U is shown in (e). Here we choose $q_x = 0.005\text{\AA}^{-1}$ and $q_y = 0$.

whole system and thus $\mathbf{M}^t = \mathbf{M}^b = \mathbf{M}$. As the strength of DM interaction is directly determined by the off-diagonal components of the spin susceptibility[23], particularly the components χ_{xz} and χ_{yz} , we next discuss the behavior of χ_{xz} in our model (χ_{yz} can be directly related to χ_{xz} due to the rotation symmetry of our model). The zero-frequency spin susceptibility is given by $\chi_{\alpha\beta}(q) = \frac{1}{\beta} \sum_{i\omega_m, k} Tr[G_0(q+k, i\omega_m)\sigma_\alpha G_0(k, i\omega_m)\sigma_\beta]$ with $\beta = \frac{1}{k_B T}$ and T is the temperature. Fig. 4(b) shows χ_{xz} as a function of asymmetric potential and chemical potential. The behavior of χ_{xz} can be understood from the energy dispersion in Fig. 4(a), which shows that the surface Dirac cones are close to the top of valence band quantum well states [24, 25]. The asymmetric potential can split the two spin states of the valence band and the surface states at the opposite surfaces. These splittings generally give rise to non-zero χ_{xz} , as shown in Fig. 4(c) for two different chemical potentials. We also notice that when the Fermi energy lies between the two spin bands of the valence quantum well states, a larger χ_{xz} can be induced, as clearly shown in Fig. 4(c), in which the red line is for $\mu = -0.02eV$ that crosses the valence band top and the blue line is for $\mu = 0.02eV$ that only crosses surface state. This is consistent with the experimental observation that the observed TH resistance is enhanced for negative back gate voltage V_b , which is expected to mainly tune the chemical potential to the valence bands. The front gate voltage V_f is expected to mainly tune the asymmetric potential U in our model and one can see from Fig. 4(c) that a large U can give rise to a strong enhancement on χ_{xz} . This is consistent with the observation in Fig. 3(b).

We note that when the chemical potential crosses only the surface states, we still see a finite χ_{xz} , but in experiments, the TH resistance almost vanishes. This is because the TH resistance can only come from the bulk carriers and it vanishes when the system is in the QAH regime with almost vanishing bulk carriers. Therefore, we also show the bulk carrier concentration ρ in Fig. 4(d) and if we assume the TH resistance is proportional to both spin susceptibility $|\chi_{xz}|^2$ and bulk carrier concentration, the behavior of TH resistance is shown in Fig. 4(e).

To summarize, we have studied the gate dependence of the THE in dual-gated magnetic TI sandwich heterostructures. We observed a crossover from the QAH effect to the THE by tuning the bottom gate, particularly under a negative bottom gate voltage. The magnitude of the THE increases with V_b because this induces an asymmetric potential between the two opposite surfaces. By applying V_t and V_b , this asymmetric potential and the mag-

nitude of the THE can be enlarged or quenched by changing the relative sign of V_t and V_b . Since the THE in magnetic TI sandwich heterostructures provides evidence of chiral magnetic domain walls, the manipulation of the THE by dual gates provides a simple way to investigate and understand chiral magnetic spin textures in real space. We note that the good correspondence between our experimental observations and theory rules against simpler explanations[26] for the THE signals in our transport measurements. Our study will also motivate more studies on nontrivial quantum phenomena in magnetic TI multilayer heterostructures and facilitate the development of the proof-of-concept TI-based spintronic devices.

ACKNOWLEDGMENTS

The synthesis of samples was supported by NSF 2DCC-MIP (DMR-1539916). The dilution electrical transport measurements were supported by DOE grant (DE-SC0019064), the Gordon and Betty Moore Foundation’s EPiQS Initiative (grant no. GBMF9063 to C.-Z. Chang), and and NSF (DMR-1707340). The electrical transport measurements above 400 mK were supported by the Institute for Quantum Matter under DOE EFRC grant DE-SC0019331. The theoretical calculations were also supported by DOE grant (DE-SC0019064).

[†]R.X., D.X. and J.J contributed equally to this work.

-
- [1] M. Z. Hasan and C. L. Kane, Colloquium: Topological insulators, [Rev. Mod. Phys. **82**, 3045 \(2010\)](#).
 - [2] X.-L. Qi and S.-C. Zhang, Topological insulators and superconductors, [Rev. Mod. Phys. **83**, 1057 \(2011\)](#).
 - [3] N. Nagaosa and Y. Tokura, Topological properties and dynamics of magnetic skyrmions, [Nat. Nanotechnol. **8**, 899 \(2013\)](#).
 - [4] F. D. M. Haldane, Model for a quantum Hall effect without Landau levels: Condensed-matter realization of the “parity anomaly”, [Phys. Rev. Lett. **61**, 2015 \(1988\)](#).
 - [5] C.-X. Liu, X.-L. Qi, X. Dai, Z. Fang, and S.-C. Zhang, Quantum anomalous Hall effect in $\text{Hg}_{1-y}\text{Mn}_y\text{Te}$ quantum wells, [Phys. Rev. Lett. **101**, 146802 \(2008\)](#).

- [6] X.-L. Qi, T. L. Hughes, and S.-C. Zhang, Topological field theory of time-reversal invariant insulators, [Phys. Rev. B](#) **78**, 195424 (2008).
- [7] R. Yu, W. Zhang, H.-J. Zhang, S.-C. Zhang, X. Dai, and Z. Fang, Quantized anomalous Hall effect in magnetic topological insulators, [Science](#) **329**, 61 (2010).
- [8] C.-Z. Chang, J. Zhang, X. Feng, J. Shen, Z. Zhang, M. Guo, K. Li, Y. Ou, P. Wei, L.-L. Wang, *et al.*, Experimental observation of the quantum anomalous Hall effect in a magnetic topological insulator, [Science](#) **340**, 167 (2013).
- [9] C.-Z. Chang, W. Zhao, D. Y. Kim, H. Zhang, B. A. Assaf, D. Heiman, S.-C. Zhang, C. Liu, M. H. Chan, and J. S. Moodera, High-precision realization of robust quantum anomalous Hall state in a hard ferromagnetic topological insulator, [Nat. Mater.](#) **14**, 473 (2015).
- [10] J. Checkelsky, R. Yoshimi, A. Tsukazaki, K. Takahashi, Y. Kozuka, J. Falson, M. Kawasaki, and Y. Tokura, Trajectory of the anomalous Hall effect towards the quantized state in a ferromagnetic topological insulator, [Nat. Phys.](#) **10**, 731 (2014).
- [11] X. Kou, S.-T. Guo, Y. Fan, L. Pan, M. Lang, Y. Jiang, Q. Shao, T. Nie, K. Murata, J. Tang, *et al.*, Scale-invariant quantum anomalous Hall effect in magnetic topological insulators beyond the two-dimensional limit, [Phys. Rev. Lett.](#) **113**, 137201 (2014).
- [12] M. Mogi, R. Yoshimi, A. Tsukazaki, K. Yasuda, Y. Kozuka, K. Takahashi, M. Kawasaki, and Y. Tokura, Magnetic modulation doping in topological insulators toward higher-temperature quantum anomalous Hall effect, [Appl. Phys. Lett.](#) **107**, 182401 (2015).
- [13] A. Neubauer, C. Pfleiderer, B. Binz, A. Rosch, R. Ritz, P. G. Niklowitz, and P. Böni, Erratum: Topological Hall effect in the A phase of MnSi, [Phys. Rev. Lett.](#) **110**, 209902(E) (2013).
- [14] M. Lee, W. Kang, Y. Onose, Y. Tokura, and N. P. Ong, Unusual Hall effect anomaly in MnSi under pressure, [Phys. Rev. Lett.](#) **102**, 186601 (2009).
- [15] N. Kanazawa, Y. Onose, T. Arima, D. Okuyama, K. Ohoyama, S. Wakimoto, K. Kakurai, S. Ishiwata, and Y. Tokura, Large topological Hall effect in a short-period helimagnet mnge, [Phys. Rev. Lett.](#) **106**, 156603 (2011).
- [16] S. X. Huang and C. L. Chien, Extended skyrmion phase in epitaxial FeGe (111) thin films, [Phys. Rev. Lett.](#) **108**, 267201 (2012).
- [17] J. Matsuno, N. Ogawa, K. Yasuda, F. Kagawa, W. Koshibae, N. Nagaosa, Y. Tokura, and M. Kawasaki, Interface-driven topological hall effect in SrRuO₃-SrIrO₃ bilayer, [Sci. Adv.](#) **2**, e1600304 (2016).

- [18] Y. Ohuchi, J. Matsuno, N. Ogawa, Y. Kozuka, M. Uchida, Y. Tokura, and M. Kawasaki, Electric-field control of anomalous and topological Hall effects in oxide bilayer thin films, *Nat. Commun.* **9**, 213 (2018).
- [19] K. Yasuda, R. Wakatsuki, T. Morimoto, R. Yoshimi, A. Tsukazaki, K. Takahashi, M. Ezawa, M. Kawasaki, N. Nagaosa, and Y. Tokura, Geometric Hall effects in topological insulator heterostructures, *Nat. Phys.* **12**, 555 (2016).
- [20] C. Liu, Y. Zang, W. Ruan, Y. Gong, K. He, X. Ma, Q.-K. Xue, and Y. Wang, Dimensional crossover-induced topological Hall effect in a magnetic topological insulator, *Phys. Rev. Lett.* **119**, 176809 (2017).
- [21] W. Wang, Y.-F. Zhao, F. Wang, M. W. Daniels, C.-Z. Chang, J. Zang, D. Xiao, and W. Wu, Chiral-bubble-induced topological Hall effect in ferromagnetic topological insulator heterostructures, *Nano Lett.* **21**, 1108 (2021).
- [22] P. Li, J. Ding, S. S.-L. Zhang, J. Kally, T. Pillsbury, O. G. Heinonen, G. Rimal, C. Bi, A. DeMann, S. B. Field, W. Wang, J. Tang, J. S. Jiang, A. Hoffmann, N. Samarth, and M. Wu, Topological Hall effect in a topological insulator interfaced with a magnetic insulator, *Nano Lett.* **21**, 84 (2021).
- [23] J. Jiang, D. Xiao, F. Wang, J.-H. Shin, D. Andreoli, J. Zhang, R. Xiao, Y.-F. Zhao, M. Kayyalha, L. Zhang, K. Wang, J. Zang, C. Liu, N. Samarth, M. H. W. Chan, and C.-Z. Chang, Concurrence of quantum anomalous Hall and topological Hall effects in magnetic topological insulator sandwich heterostructures, *Nat. Mat.* **19**, 732 (2020).
- [24] C.-Z. Chang, W. Zhao, D. Y. Kim, P. Wei, J. K. Jain, , C. Liu, M. H. W. Chan, and J. S. Moodera, Zero-field dissipationless chiral edge transport and the nature of dissipation in the quantum anomalous Hall state, *Phys. Rev. Lett.* **115**, 057206 (2015).
- [25] W. Wang, Y. Ou, C. Liu, Y. Wang, K. He, Q.-K. Xue, and W. Wu, Direct evidence of ferromagnetism in a quantum anomalous Hall system, *Nat. Phys.* **14**, 791 (2018).
- [26] K. M. Fijalkowski, M. Hartl, M. Winnerlein, P. Mandal, S. Schreyeck, K. Brunner, C. Gould, and L. W. Molenkamp, Coexistence of surface and bulk ferromagnetism mimics skyrmion Hall effect in a topological insulator, *Phys. Rev. X* **10**, 011012 (2020).